Theoretical Prediction of the Rate Constants for Exciton Dissociation and Charge Recombination to a Triplet State in PCPDTBT with Different Fullerene Derivatives

ARTICLE *in* THE JOURNAL OF PHYSICAL CHEMISTRY C · JANUARY 2014

Impact Factor: 4.77 · DOI: 10.1021/jp410562u

4 AUTHORS, INCLUDING:

Yubing Si
Xiamen University
20 PUBLICATIONS **105** CITATIONS
SEE PROFILE

Yi Zhao
Xiamen University
87 PUBLICATIONS **1,159** CITATIONS
SEE PROFILE

THE JOURNAL OF PHYSICAL CHEMISTRY C

Article

pubs.acs.org/JPCC

Theoretical Prediction of the Rate Constants for Exciton Dissociation and Charge Recombination to a Triplet State in PCPDTBT with Different Fullerene Derivatives

Can Leng, Haimei Qin, Yubing Si, and Yi Zhao*

State Key Laboratory of Physical Chemistry of Solid Surfaces, Collaborative Innovation Center of Chemistry for Energy Materials, Fujian Provincial Key Lab of Theoretical and Computational Chemistry, and College of Chemistry and Chemical Engineering, Xiamen University, Xiamen 361005, P. R. China

Supporting Information

ABSTRACT: The exciton dissociations and charge recombinations to a triplet state in the donor−acceptor heterojunction solar cells of [2,6-(4,4-bis(2-ethylhexyl)-4*H*-cyclopenta-[2,1-b;3,4-b]dithiophene)-*alt*-4,7-(2,1,3-benzothiadiazole)] (PCPDTBT) blended with ten different fullerene derivatives are theoretically investigated by using electronic structure calculations together with a Marcus formula. The detailed discussions of available accuracy in the evaluation of all quantities entering the rate expression (driving force, electronic coupling, and internal and external reorganization energies) are provided. The results reveal that the exciton dissociations in most blends are barrierless reactions because the corresponding values of driving forces and reorganization energies are very close; however, the recombinations from the charge transfer states to the triplet state of PCPDTBT occur in the Marcus normal regime. The predicted rates for both the exciton dissociation and charge recombination are in quite good agreement with experimental measurements. In addition, as the triplet charge transfer states are formed, their recombination rates become two orders larger than those for the singlet ones and have orders similar to the exciton dissociations. It is thus expected that the triplet charge recombinations are dominant channels, whereas the singlet charge recombinations can be safely neglected because of quite small rates compared to exciton dissociation ones.

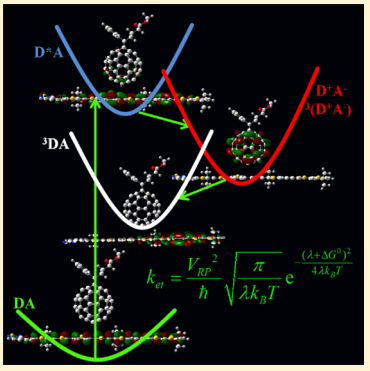

1. INTRODUCTION

Low-bandgap polymers represent a promising way to increase the power conversion efficiency (PCE) of organic bulk heterojunction (BHJ) solar cells.[1−3] They are able to absorb a larger portion of the solar spectrum than conventional conjugated polymers and efficiently enhance the short-circuit current density. Polycyclopentadithiophene-benzothiadiazole (PCPDTBT) is a typical low-bandgap polymer, consisting of an electron-rich (cyclopentadithiophene, CPDT) and an electron-poor (benzothiadiazole, BT) units. Since the PCPDTBT has been used as a donor (D) in BHJ solar cells,[4] it is getting much attention due to its ideal band gap with a spectral response that extends to 900 nm, excellent absorption, and charge carrier properties. As reported, the PCE of PCPDTBT blended with the acceptors (A) of fullerene derivatives has been over 2.7% and later achieved 5.5% by the morphology control in device fabrication processes.[4−8]

It is known that the PCE is dominantly determined by the photophysical processes occurring in the BHJ solar cells, and the basic steps of those processes are now clear. After a donor absorbs sunlight, an exciton in the excited state is generated and subsequently dissociated to a Coulomb-bounded electron−hole pair in the charge transfer (CT) state when it migrates to the interface of the donor−acceptor. The bounded electron−hole pair may either separate to free charge carriers or recombine radiatively or nonradiatively to the ground state (S_0). Therefore, the structures of the solar cells with the high PCE should make the exciton dissociation as high as possible and charge recombination as little as possible. In the solar cells of PCPDTBT with fullerene derivatives,[7−11] besides those recombination channels to the ground state, the populated CT state can decay via the triplet excited state (T_1) of the blend (see, for instance, ref 12, and references therein), which limits the attainable PCE. This phenomenon has also been found in other polymers, such as dicyanovinyl-substituted oligothiophenes (DCV_nT),[13] poly(9,9-dioctylfluorene-*alt*-benzothiadiazole) (F_8BT),[14] 1-[3-(2-ethyl)hexoxy carbonyl]propyl-1-phenyl-$Lu_3N@C_{80}$ ($Lu_3N@C_{80}$-PCBEH),[15] and poly(indace-nodithiophene-*co*-phenanthro[9,10-b]-quinoxaline) (PIDT-PhanQ).[16]

It has been highlighted that the charge recombination via triplet states can be suppressed whenever the energies of the T_1 states are above that of the interfacial CT state. Indeed, several studies[7,14,15,17−23] have confirmed this mechanism by controlling the morphology of the film and molecular doping to modify the energy of the CT state. However, the contradictive phenomenon has also been reported.[16,24] For instance, Schlenker et al.[16] have observed the efficient photocurrent

Received: October 25, 2013
Revised: December 31, 2013
Published: January 3, 2014

   dx.doi.org/10.1021/jp410562u | J. Phys. Chem. C 2014, 118, 1843−1855

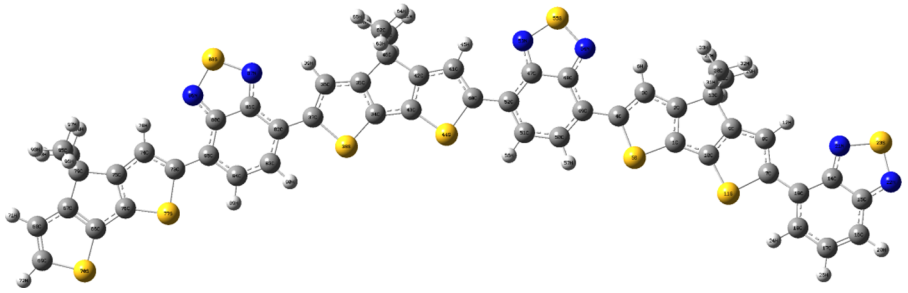

Figure 1. Optimized S_0 geometric structure of the PCPDTBT at the CAM-B3LYP/6-31G* level of theory.

collection at short circuit and a reasonable fill factor, which can be maintained even in the case that the lowest interfacial CT state is several hundred millielectronvolts higher in energy than the triplet state of the donor polymer PIDT−PhanQ blended with phenyl-C_{70}-butyric acid methyl ester ($PC_{70}BM$). Essentially, the exciton dissociation and charge recombination are nonadiabatic processes. Therefore, the energy gap is not a unique factor to determine the corresponding rates, and the electronic coupling (V) between two diabatic states and reorganization energy (λ) are also equally important. In the present work, we theoretically predict the rates of the exciton dissociation and charge recombination via the triplet state in the PCPDTBT with a variety of fullerene derivatives to reveal their photophysical processes.

From a theoretical point of view, the exciton dissociation and charge recombination can be treated as the nonadiabatic reactions occurred between two parabolic potentials. In this case, the well-known semiclassical Marcus formula[25,26] becomes suitable to estimate their rates, although several more general approaches are available (see, for instance, ref 27, and references therein). Indeed, the Marcus formula together with electronic structure calculations have already been applied to successfully predict the CT rates in several BHJ solar cells.[3,28−36] To predict the rates from the Marcus formula, one has to know the following three factors: the driving force ΔG, reorganization energy λ, and electronic coupling V. For the photoinduced CT in the present donor−acceptor systems, however, the rigorous electronic structure calculations for those factors still meet challenges because the structure information of the local excited state and CT state of the blends is required. We thus adopt popular approximation models, such as the Rehm−Weller expression[37] for ΔG and the four-point model for λ,[38] as well as the wave function overlap for V. However, we will carefully demonstrate the accuracy of calculations for those parameters from the experimental absorption and fluorescence spectra. Then, we propose possibly favorable candidates of acceptors from the predicted rates of the exciton dissociation and charge recombination in PCPDTBT with several fullerene derivatives.

It is interestingly noted that the coherent motion of charge carriers generated from the high-energy photoexcitation has been recently observed to enhance charge separation and suppress recombination.[24,39−42] For example, Rao et al.[24] have reported in the blends of PIDT−PhanQ with several fullerene derivatives that even when energetically favored from the CT states to the T_1 state the corresponding recombinations are strongly suppressed by the wave function delocalization of hole, allowing that the electron−hole pairs forwardly transfer from the CT state to the charge separation state, and the high yield of free charge carriers is finally achieved. The hot populated CT states are also proposed to efficiently enhance the charge separation.[18,41−43] Although the description of detailed coherent dynamics needs device-physical models,[44,45] which is beyond this work, the present investigation can still qualitatively judge the possibility of the coherent motions because the relative magnitudes of electronic coupling and reorganization energy essentially determine the band-like or hopping-type mechanism of carrier motions. Furthermore, it has been shown[46] that the bimolecular and germinate recombinations have the same mechanism as the electron−hole pairs meet each other at the donor−acceptor interface. Therefore, the rate is still a key factor to control the recombination processes for both coherent and incoherent carrier motions.

The paper is arranged as following. Section 2 displays the geometries and electronic properties of PCPDTBT/fullerene derivatives. Sections 3 and 4 show the rates for exciton dissociation and charge recombination, respectively, and the concluding remarks are shown in Section 5.

2. STRUCTURES AND ELECTRONIC PROPERTIES OF PCPDTBT AND FULLERENE DERIVATIVES

In the BHJ solar cells, fullerene derivatives are commonly used as acceptors because of their high electron affinity and reasonable good electron mobility. Since the solar cell is first reported with the soluble fullerene derivative as an acceptor,[47] a large quantity of BHJ solar cells have been constructed with a variety of fullerene derivatives. For the present purpose, we choose the following ten fullerene derivatives:[48−50] $IC_{60}BA$, $bisPC_{70}BM$, $PC_{60}BM$, $PC_{70}BM$, F_9, F_{16}, F_1, F_{33}, F_2, and F_{12}. The reason is that their open circuit voltage (V_{OC}) blended with the state-of-the-art P_3HT polymer has been measured,[48,49] which can be applied to validate the present calculations. We summarize the values of V_{OC} and display them in Figure S1 of the Supporting Information (SI). Furthermore, the PCPDTBT with $PC_{60}BM$ and $PC_{70}BM$ among those derivatives are already used to perform highly efficient BHJ solar cells experimentally.[5,22,42,51−55] This motivates us to find out whether the PCE can be further raised with the other fullerene derivatives.

In the electronic structure calculations of PCPDTBT, the previous investigations[3,35,56−59] have shown that the density functional theory (DFT) with different functionals predicts very similar geometry, but the excited-state energies heavily depend on the functionals in the time-dependent (TD) DFT. From our previous work,[60] it is expected that the CAM-B3LYP[61] and ωB97XD[62] may apply because they are suitable to calculate the excitation energies for the charge-delocalized systems. Indeed, Fischer et al.[57] have shown that the low-energy excited state (S_1) of the PCPDTBT predicted from the CAM-B3LYP level is

dx.doi.org/10.1021/jp410562u | J. Phys. Chem. C 2014, 118, 1843−1855

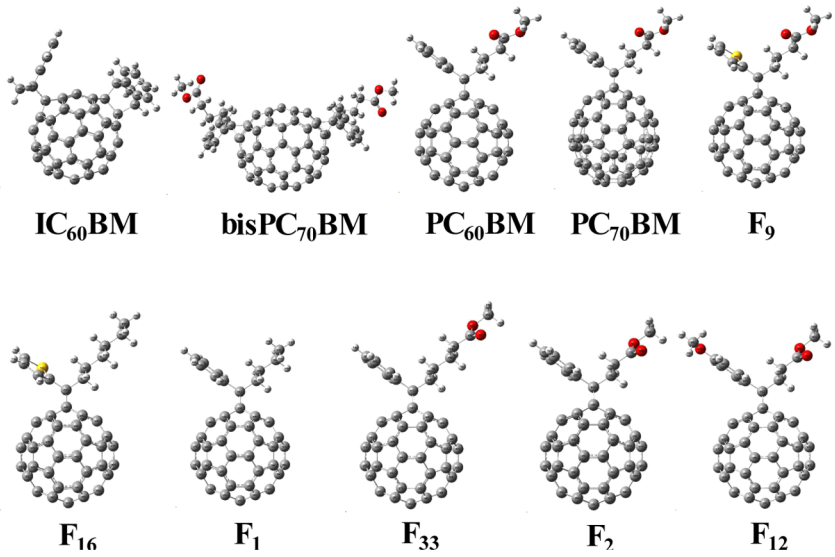

Figure 2. Optimized S_0 geometric structures of ten fullerene derivatives at the B3LYP/6-31G* level of theory.

Table 1. AEA and Effective Radius d_A of A Molecules, the Center of Mass Distances R_{DA} between D and A Molecules, the Coulomb Interactions E_{coul} between D^+ and A^- Molecules, and the Driving Forces ΔG_{CT1} between D*A and D^+A^- States and ΔG_{CT2} between D*A and (D^+A^-)*[a]

	$IC_{60}BA$	$bisC_{70}BM$	$PC_{60}BM$	$PC_{70}BM$	F_9	F_{16}	F_1	F_{33}	F_2	F_{12}
AEA	3.15	3.19	3.35	3.34	3.36	3.36	3.34	3.35	3.36	3.34
d_A	3.48	3.37	3.59	3.94	3.59	3.59	3.59	3.59	3.59	3.59
R_{DA}	3.10	3.20	3.10	3.10	3.10	3.10	3.10	3.10	3.10	3.10
E_{coul}	−0.163	−0.338	−0.361	−0.354	−0.352	−0.336	−0.363	−0.351	−0.347	−0.339
ΔG_{CT1}	−0.001	−0.217	−0.398	−0.384	−0.406	−0.614	−0.396	−0.387	−0.395	−0.373
ΔG_{CT2}	0.279	−0.167	−0.338	−0.314	−0.346	−0.565	−0.336	−0.327	−0.344	−0.313

[a]Units of energy is eV, and the distance is in Å.

about 1.83 eV, whereas it becomes 1.02 eV from the B3LYP level which is strongly underestimated from the experimental value of 1.68 eV in chlorobenzene. The reason is that the calculated excitation energies are larger with a larger Hatree−Fock exchange percent in functionals.[60] Therefore, we adopt the CAM-B3LYP/6-31G*, which is most used in the previous reports,[35,57−59] to optimize the geometries of the S_0, T_1, and ionic structures of the PCPDTBT. In addition, since we focus on the CT state in the PCPDTBT blended with fullerene derivatives, the static electric field from their films may have an influence on the molecular geometries and energies. This effect is further mimicked by using the Polarizable Continuum Model (PCM). It is noted that even for the $P_3HT/PC_{60}BM$ blend the dielectric constant from the experiments is in the range of 3.4−4.[54,63] We think that the different dielectric constant might come from the different aggregation. In the present calculations, therefore, we use the up-limit of dielectric constants from the experiments to mimic the aggregation effect of blends (3.9 is from the blend of PCPDTBT/$PC_{70}BM$[64]). All the calculations are implemented with the PCM in the Gaussian 09 program.[65]

Figure 1 displays the optimized geometry of the S_0 state of the PCPDTBT with three CPDTBT units as a model. This geometry is similar to the one in the gas phase and consistent with previous reports.[35,57] It is noted that a different isomerized geometry of PCPDTBT has also been investigated,[58,59] but the PCPDTBT for these two isomerized structures has similar photophysical properties.[35] The obtained vertical excitation energy to the S_1 state and the corresponding adiabatic excitation energy are 2.16 and 1.89 eV, respectively, and the energy of optimized T_1 is 1.08 eV. Although the vertical excitation energy is larger than the experimental one, its asymptotic value with the infinite CPDTBT units is close to the experimental measurement of 1.0 eV.[7] The adiabatic ionization potential (AIP) predicted from the CAM-B3LYP is 5.0 eV which is also in the range of the experimental data of 5.0−5.3 eV.[66,67] These calculations manifest that three CPDTBT units may represent the most important electronic and photophysical properties of the PCPDTBT. Therefore, in the present BHJ model, the PCPDTBT with three CPDTBT units is used as the donor, and it is expected that similar trends in the calculations of the dissociation and recombination rates should be obtained with use of larger units of CPDTBT and higher level of electronic structure calculations.

Now, we focus on the fullerene derivatives. Because of their sphere structures, the popular B3LYP is still a good choice for their electronic structure calculations.[68] In the present calculations, the B3LYP/6-31G* is used in the geometric optimizations, and the energies are further corrected by the B3LYP/6-311G**. Figure 2 displays the optimized geometries of the S_0 states for ten fullerene derivatives, which are consistent with the experimental geometries.[48,49] For those derivatives, the adiabatic electronic affinity (AEA) energies are very important because they determine the driving force for the exciton dissociation at the interface. Although the highest occupied molecular orbital (HOMO) and the lowest unoccupied molecular orbital (LUMO) energies, in general, track well the AIP and AEA, respectively, the calculated AEA

dx.doi.org/10.1021/jp410562u | J. Phys. Chem. C 2014, 118, 1843−1855

should be closer to experimental values. Table 1 lists the AEA predicted from the B3LYP/6-311G** in the medium with ε = 3.9, and Figure 3 displays the corresponding values in both the

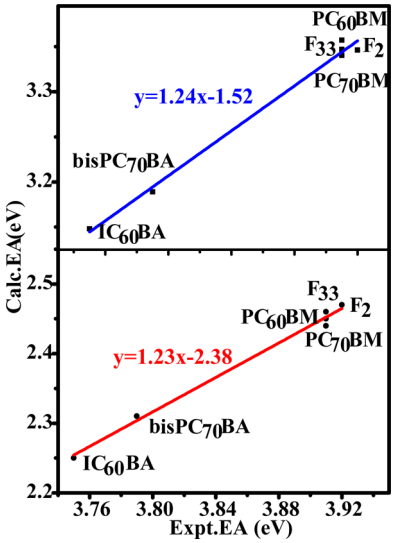

Figure 3. Calculated adiabatic electronic affinities in the referring solvent (blue line) and vacuum (red line) with respect to experimental measurements.

solvent and vacuum with respect to the experimental measurements.[48−50] It is seen that the values of AEA in vacuum are much smaller than those in the solvent. However, both values are underestimated compared to the experimental values. The larger AEAs of the experiments may correspond to the aggregated effect because the different AEAs are reported in different morphology.[69,70] However, there is a good linear relationship between the experimental and theoretical values. From this relationship, it is easy to estimate the AEAs of fullerene derivatives which are not available experimentally. For instance, from the calculated AEAs of F_9, F_{16}, F_1, and F_{12}, shown in Table 1, the estimated experimental values should be 3.93, 3.92, 3.91, and 3.91 eV, respectively, which need to be confirmed by further experiments.

As the PCPDTBT and fullerene are blended together, one has to know their arrangements at the interface. The previous works for other BHJ solar cells have shown that the arrangements are very important to determine the PCE. For instance, Liu et al.[71] have investigated eight possible orientations between polymer P_3HT_6 and $PC_{60}BM$, and Yi et al.[29] have used two orientations with donor perpendicular or parallel as an acceptor in a pentacene/fullerene system. It is found that the different arrangements dominantly affect the electronic couplings for the exciton dissociations. For the present purpose, we use a favorable arrangement with a large electronic coupling,[71] in which the polymer's carbon−carbon bond is perpendicular with the six-carbon ring's carbon−carbon bond of fullerenes. To find the optimized mass-center distances between the PCPDTBT and fullerene derivatives, we have calculated the potential energy curves along the mass-center distance, and the minimal potentials can be indeed found in the blends. As an example, Figure 4 displays the potential energy curve with respect to the distance between the PCPDTBT and $PC_{60}BM$. It is seen that the potential energy curve nearly has a Morse potential form, and the optimized distance is 3.1 Å. The other optimized distances are listed in Table 1, and they are

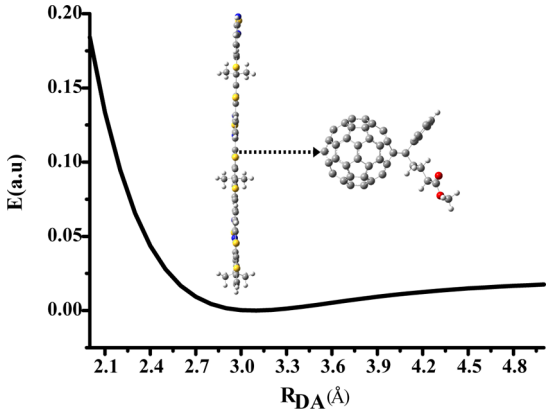

Figure 4. Potential energy curve of $PCPDTBT_3/PC_{60}BM$ with respect to the distance between $PCPDTBT_3$ and $PC_{60}BM$.

very close to one another in the range of 3.1−3.2 Å. In the following rate calculations, these geometries with the minimum potentials are adopted as the interface arrangements.

3. EXCITON DISSOCIATION

After an exciton in the donor PCPDTBT is generated from photoexcitation and migrates to the interface between the PCPDTBT and the acceptor fullerene derivatives, it may dissociate into an electron and a hole. The electron will transfer to the fullerene derivatives because of the strong AEA, whereas the hole still stays in the PCPDTBT. Starting from the states of D and A molecules, the exciton dissociation can be thought of as a nonadiabatic reaction from the initial state D*A to the final state D^+A^-, where D* represents the excited state of the D molecule and D^+ and A^- are the ionic states of D and A molecules, respectively. As the vibrational frequencies of states D*A and D^+A^- along the reaction coordinate are close to each other, the reorganization energy λ can be introduced, as shown in Figure 5, in which ΔG is the driving force. In this case, the

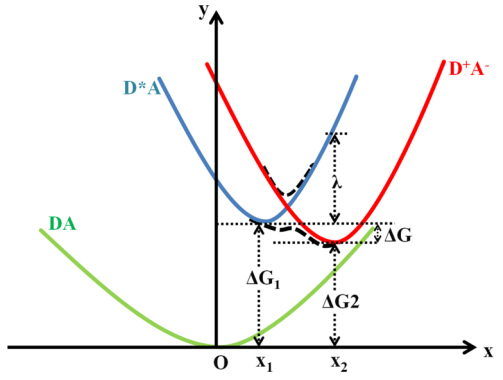

Figure 5. Schematic potential energy profile for exciton dissociation.

exciton dissociation rate is given by the well-known Marcus formula[25,26]

$$k = \frac{|V|^2}{\hbar}\sqrt{\frac{\pi}{\lambda k_B T}}\exp\left(-\frac{(\lambda + \Delta G)^2)}{4\lambda k_B T}\right) \quad (1)$$

where V is the electronic coupling between the D*A and D^+A^- states and T is temperature. To predict the rate, therefore, one has to know λ, ΔG, and V.

dx.doi.org/10.1021/jp410562u | J. Phys. Chem. C 2014, 118, 1843−1855

Before their calculations, we consider that the photoabsorption property after the PCPDTBT is blended with fullerenes. As mentioned above, the excited states of PCPDTBT themselves show charge delocalization, whereas the blends may have a charge localization property because of the CT states. The functionals in the TDDFT calculations should describe both the charge localization and delocalization. To find a suitable functional, we use the hybrid to long-range functionals to calculate the vertical excitation energies and the corresponding oscillator strengths of the PCPDTBT/$PC_{60}BM$ in the solvent with ε = 3.9 (shown in Figure S2 in SI). It is found that the lowest excitation of the blend, predicted from long-range functionals CAM-B3LYP, M06HF, and LC-ωPBE, dominantly comes from the S_0 to S_1 contribution of PCPDTBT, whereas it becomes a CT state with a relative small oscillator strength from the hybrid functionals of B3LYP and MP1PW91. However, the experimental spectra do not show obvious CT absorption in the low-frequency domain.[8,42] It is thus expected that only the long-range functionals can correctly describe the photoabsorption property of the blends. Although the predicted low-lying excitations from the different long-range functions have explicitly different energies, they have similar photophysical properties: $S_0 \rightarrow S_1$ corresponds to the first excited-state absorption of PCPDTBT, and $S_0 \rightarrow S_2$ and $S_0 \rightarrow S_3$ are two CT absorptions of the blend with slightly higher energies. To be consistent with the calculations of PCPDTBT, we still adopt the CAM-B3LYP in the excitation calculations of blends. Figure 6 displays the low-lying three excitations of the

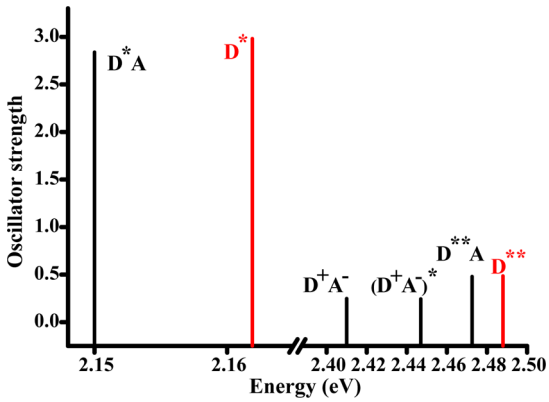

Figure 6. Oscillation strengths of vertical excitations in the PCPDTBT (red line) and PCPDTBT/$PC_{60}BM$ molecules (black line) at the CAM-B3LYP/6-31G* level. D*A refers to S_1; two CT absorption D^+A^- and (D^+A^-)* refer to S_2 and S_3, respectively; D**A refers to S_4; D* and D** refer to the first and second excited state S_1 and S_2 of polymer PCPDTBT, respectively.

PCPDTBT/$PC_{60}BM$, as well as those for the PCPDTBT itself, and Figure 7 is the corresponding molecular orbitals. Interestingly, the $S_0 \rightarrow S_1$ excitation in the blend comes from the HOMO to LUMO+3 transition other than the HOMO to LUMO as in the PCPDTBT. Two CT absorptions from S_0 to S_2 and S_3 are corresponding to the transitions from the HOMO-2 to LUMO and HOMO-2 to LUMO+1, respectively. However, the direct CT state excitations have quite small oscillation strengths compared to the first excitation; therefore, the CT states are dominantly created by the exciton dissociation. In the following, we present the calculations for the parameters to determine the rate of exciton dissociation.

3.1. Driving Force. The driving force ΔG is the adiabatic energy difference of two diabatic D^+A^- and D*A states, as shown in Figure 5. However, it still meets a challenge to obtain these optimized states in the present electronic structure calculations. As an approximation, ΔG is commonly estimated from the Rehm–Weller equation[37]

$$\Delta G = E(D^+/D) - E(A/A^-) - \Delta E_{00} - \frac{1}{4\pi\varepsilon_r\varepsilon_0} \sum_{i\in D^+}\sum_{j\in A^-}\frac{q_i q_j}{r_{ij}} \quad (2)$$

where $E(D^+/D)$, $E(A/A^-)$, and E_{00} correspond to the AIP of the isolated donor, the AEA of the isolated acceptor, and the adiabatic energy difference of the D*A and DA states, respectively, and the last term represents the Coulomb interaction. The AIP of PCPDTBT and AEA of fullerene derivatives have been extensively discussed in Section 2, and the calculated values can be straightforwardly used here.

In the Coulomb interaction term, one needs to know the atomic charges q_i in the D and A molecules. Earlier attempts[72−75] have used the point charge model to estimate the Coulomb interaction as the distance of the D and A moleculars is large enough. For the present components, the optimized distances are about 3.2 Å, which have magnitude similar to the sizes of D and A and are even smaller than the length of the polymer chain. We therefore subtract the atomic charge distributions from the electronic structure calculations to estimate the Coulomb interaction. In the present electronic structure theory, there are a variety of analyses for charge population distributions,[76] such as Mulliken,[77,78] NPA,[79,80] Hirshfeld,[81] CHELPG,[82] and Merz–Kollman (MK).[83,84] It is not clear which is the best one to describe the Coulomb interaction in the driving force. Fortunately, it has been demonstrated experimentally that the V_{OC} displays a linear relationship with the energy gap between the ionization potential (IP) of the donor and electronic affinity (EA) of the acceptor,[85−87] which are the determination of the driving force, thus we can illustrate this problem by comparing ΔG calculated from different charge population analyses with the experimental V_{OC}. To do so, we take the P_3HT_6/fullerene derivatives as model systems because the measured V_{OC} are available.[49] Among the calculated Coulomb interactions from the above five charge analyses, shown in Figure S3 in the SI, the charges from the MK and CHELPG analysis predict obviously smaller Coulomb interactions than the other charge analyses and even a repulsive interaction for $P_3HT_6/PC_{70}BM$. Therefore, we only calculate the ΔG from the other three charge analyses, and the calculated ΔG with respect to the measured V_{OC} are shown in Figures S4–S6 in the SI. The results reveal that ΔG from the NPA and Hirshfeld charge distributions have a better linear relationship with V_{OC} than the Mulliken charge distribution. The possible reason has been illustrated by the previous investigations.[76] In the present work, therefore, we use the NPA charge distribution to get the Coulomb interaction between the PCPDTBT and fullerene derivatives, and the obtained Coulomb interactions are listed in Table 1.

The adiabatic energy gap E_{00} between D*A and DA needs the excited-state calculations. It may be approximately estimated from the gap of donor D because the interaction between D and A is expected to be weak, which has been demonstrated by the absorption spectra in Figure 6. Even in this simple case, it is not easy to accurately obtain the optimized

dx.doi.org/10.1021/jp410562u | J. Phys. Chem. C 2014, 118, 1843−1855

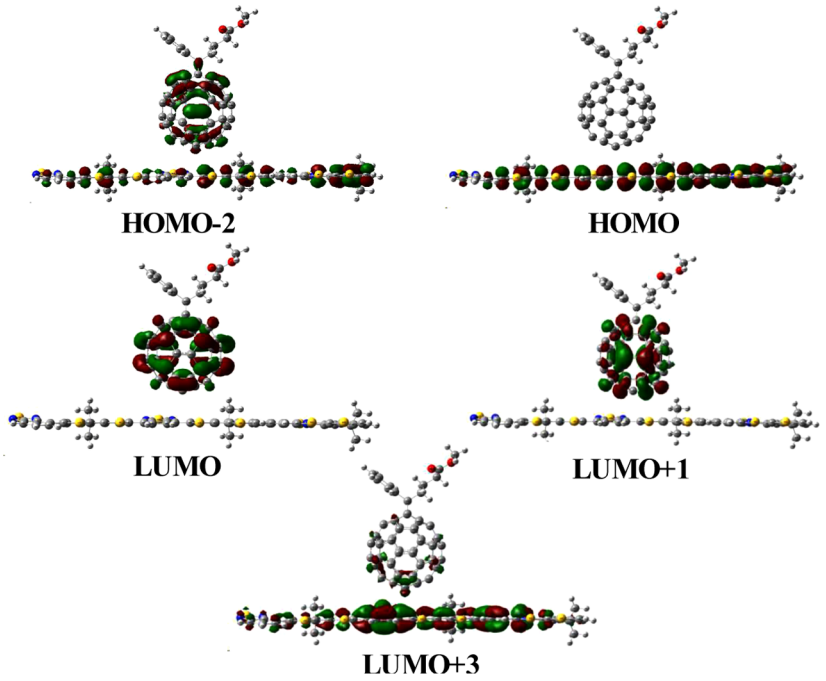

Figure 7. Molecular orbitals of the PCPDTBT/$PC_{60}BM$ molecule in the CAM-B3LYP/6-31G* level.

excited-state energy of PCPDTBT from the TDDFT calculations. Here, we estimate it from the experimental emission spectral energy by adding the ground-state energy difference at the optimized excited-state and ground-state geometries because the calculated ground-state energies are relatively accurate in the present DFT calculations. The CAM-B3LYP/6-31G* predicts 0.27 eV for this ground-state energy difference. Together with experimental emission energy of 1.42 eV,[8,42] the obtained E_{00} is 1.69 eV, which is 0.20 eV smaller than that from the straightforward calculation.

The driving force ΔG_{CT} now can be obtained from the above calculated values, and results are listed in Table 1, in which the driving forces ΔG_{CT2} between D*A and the second CT state of (D^+A^-)* are estimated from ΔG_{CT1} by adding the energy gaps of LUMOs with respect to the corresponding excitations. Figure 8 displays the energies of D*A and the first D^+A^- states. It is seen that the driving forces are positive for $IC_{60}BA$, which

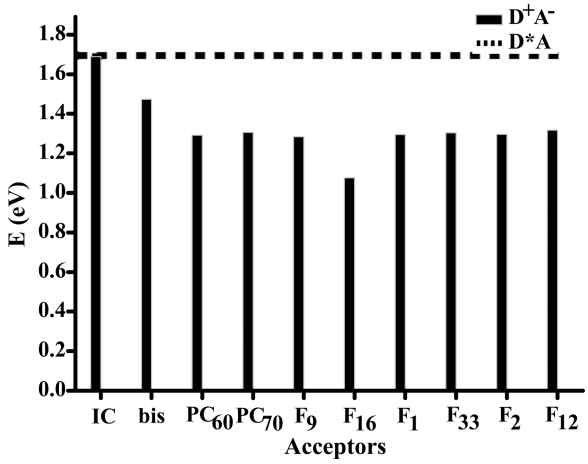

Figure 8. Energies of D^+A^- and D*A states. The driving forces correspond to the energy gaps of these two states.

may be caused by the small AEAs of these two derivatives. For the $IC_{60}BA$, the Coulomb interaction is only about half compared to others because of missing the electrophilic group in the side chain, which leads to a more positive value of ΔG_{CT1}. In all the derivatives, F_{16} has the lowest value of ΔG_{CT1}.

It is known that the driving force is closely related to the emission spectra energies of D*A and D^+A^- states, which can be used to judge the accuracy of the present calculations. For the blend of PCPDTBT and $PC_{60}BM$, the experimental emission energies are 1.42 and 1.15 eV for D*A and D^+A^- states, respectively.[8,42] The corresponding driving force should be larger than 1.15 − 1.42 = −0.27 (eV). Indeed, the calculated value of −0.39 eV is consistent with the experimental estimation of −0.27 eV. Furthermore, we can estimate the CT emission energy from the calculated adiabatic energy of the CT state (1.29 eV). To do it, we calculate the neutral blend energy at the D^+A^- geometry, and the result is 0.28 eV. Then, the theoretically predicted CT emission energy should be 1.29 − 0.28 = 1.01 (eV), very close to the experimental value. These good agreements between experimental and theoretical values manifest that the Rehm−Weller equation is reasonable to estimate the driving force once the AIP, AEA, and Coulomb interactions are accurately estimated.

3.2. Reorganization Energy. The reorganization energy is normally decomposed into internal (vibrational reorganization energy λ_{in}) and external (solvent λ_s) contributions. The former arises from the changes in the geometry of the donor and acceptor moieties and the latter from changes in the electronic and nuclear polarization of the surrounding medium upon charge transfer. An easy way to calculate the internal reorganization energy is the four-point technique proposed by Nelsen[38] which has been identified as a reliable tool.[88,89] Concretely, with use of n and c to represent the optimized geometries of the neutral and cationic components, and the charge labeled as the superscript, the reorganization energy is given by[38,90]

dx.doi.org/10.1021/jp410562u | J. Phys. Chem. C 2014, 118, 1843−1855

$$\lambda_{in} = [E(c^0) - E(n^0)] + [E(n^+) - E(c^+)] \quad (3)$$

where E are the corresponding energies. In eq 3, it is assumed that the precursor pair is n^0, c^+, and the Franck−Condon excited states are c^0, n^+, respectively. We use this technique to calculate λ_{in} between the D*A and D^+A^- states, and the obtained results for all ten derivatives are listed in Table 2.

Table 2. Reorganization Energies for D*A → D^+A^- from Two-Sphere Model Calculations (eV)

	equilibrium solvent			nonequilibrium solvent
systems	λ_{in}	λ_s	λ_1	λ_2
PCPDTBT-IC_{60}BM	0.1071	0.2956	0.4027	0.4090
PCPDTBT-bisC_{70}BM	0.0756	0.2945	0.3701	0.3674
PCPDTBT-PC_{60}BM	0.1036	0.2945	0.3981	0.4102
PCPDTBT-PC_{70}BM	0.1152	0.2824	0.3976	0.4160
PCPDTBT-F_9	0.1043	0.2919	0.3962	0.4089
PCPDTBT-F_{16}	0.1025	0.2919	0.3944	0.4073
PCPDTBT-F_1	0.1026	0.2919	0.3945	0.4082
PCPDTBT-F_{33}	0.1036	0.2919	0.3955	0.4087
PCPDTBT-F_2	0.1026	0.2919	0.3945	0.4074
PCPDTBT-F_{12}	0.1028	0.2919	0.3947	0.4079

The accurate calculation of external reorganization energy is still not easy work. Although several modern methods combining quantum mechanics and molecular mechanics have been proposed (for instance, see ref 91 and references therein), an easy way is still the"two-sphere model" based on the continuum medium model,[92] and it predicts λ_s as follows

$$\lambda_s = \Delta q^2 \left(\frac{1}{2d_D} + \frac{1}{2d_A} - \frac{1}{d_{DA}}\right)\left(\frac{1}{\epsilon_{op}} - \frac{1}{\epsilon_o}\right) \quad (4)$$

where d_D, d_A, and d_{DA} are donor, acceptor radius, and the mass-center distance between the donor and acceptor, respectively. ϵ_{op} and ϵ_o are optical and zero-frequency dielectric constants of the surrounding media, respectively. Empirically, the effective radius of the donor and acceptor is calculated as the radius of the molecule sphere volume defined as the volume inside a contour of 0.001 electrons/$bohr^3$ density,[93,94] implemented by the PCM model in Gaussian 09. However, the chain of PCPDTBT is too long to map it as to a point charge sphere. Here, the distances with the minimized energies (R_{DA} in Table 1) are approximated to be the values of d_D. Except PC_{70}BM, bisPC_{70}BM, and IC_{60}BA, other fullerene derivatives have similar geometries, and the same radii are thus used. The corresponding d_A's are listed in Table 1. The distance d_{DA} is the simple sum of d_D and d_A. With the use of ϵ_{op} = 2.56 and ϵ_o = 3.90, we can obtain the solvent reorganization energies λ_s, as listed in Table 2.

On the basis of the concept of equilibrium and non-equilibrium solvation free energies,[95] alternatively, the four-point model can be straightforwardly used to calculate the total reorganization energy with use of the nonequilibrium solvent. The implementation detail is the same as that in the calculation of internal reorganization energy, but the molecular energies of the Franck−Condon excited states are calculated from the nonequilibrium solvents which are in equilibrium with the molecular ground state densities. The implicit mechanism is the linear response theory that predicts a harmonic potential along the solvent reaction coordinates. The calculated total reorganization energies with use of the PCM model in Gaussian 09 are listed in Table 2.

This table clearly shows that the total reorganization energies λ from both techniques are surprisingly consistent. It manifests that the two-sphere model is still a good and easy way to calculate the solvent reorganization once the molecular radius is reasonable. To avoid the error of radius used, the reorganization energies from the nonequilibrium solvent method are adopted in the rate calculations.[95] Interestingly, the magnitudes of the total reorganization energies for the ten fullerene derivatives are very close, and they are about 0.41 eV, not far from the previous estimation of 0.50 eV.[29,75] Moreover, total reorganization energies are dominated by the solvent ones because internal reorganization energies are only about 0.1 eV, which may be explained by the small geometric change from the excited state to the ionic state.

3.3. Electronic Coupling. Compared to the reorganization energy calculation, the accurate method to calculate the electronic coupling is not well established yet, although a number of approximated approaches have been proposed,[96] such as Koopmans' theorem (KT) method,[97−100] the two-state model (TM),[101] the spin-flip (SF) strategy,[102,103] the generalized Mulliken−Hush (GMH) method,[104] and the reduced TM (RTM).[105,106] From our previous experiences,[27,60,89,106−108] the RTM should be suitable for the present systems because the exciton and CT states are well represented by the single molecular orbitals (see Figure S7 in SI and Figure 7).

Similar to the TM, the RTM predicts the electronic coupling by the overlap of the two diabatic states, but the diabatic states are assumed to be the LUMOs of two isolated neutral molecules, leading to a secular equation

$$\begin{pmatrix} h_{11} & h_{12} \\ h_{12} & h_{22} \end{pmatrix} C = E \begin{pmatrix} 1 & S_{12} \\ S_{21} & 1 \end{pmatrix} C \quad (5)$$

where $h_{ij} = \langle \phi_i | h_{KS} | \phi_j \rangle$, $S_{ij} = \langle \phi_i | S | \phi_j \rangle$, and $|\phi_i\rangle$ (i = 1,2) is the electronic wave function of LUMO for the i-th molecule. These quantities can be calculated from the Kohn−Sham (KS) equation. After the transformation of eq 5 into the orthogonal basis set, the electronic coupling is given by

$$V_{DA} = \frac{h_{12} - 12(h_{11} + h_{22})S_{12}}{1 - S_{12}^2} \quad (6)$$

In the present systems, the electronic densities in the two CT states are well localized on the polymer and fullerene derivatives. Therefore, the electronic couplings between the LUMO of PCPDTBT and LUMO and LUMO+1 of fullerene derivatives can be used for exciton dissociations. In the calculations, the M06HF is adopted because it is well suitable for the charge-localized systems in the electronic coupling calculaitons.[60]

The calculated electronic couplings for both the exciton dissociation channels are listed in Table 3. It is found that the electronic couplings have a similar order for both the channels, manifesting that the two channels should be equally important for exciton dissociation. Furthermore, their values are quite small compared to the reorganization energies, and the Marcus formula is expected to be suitable for the estimation of the rates.

3.4. Exciton Dissociation Rates. From the obtained ΔG, λ, and V, the exciton dissociation rate can be easily estimated

dx.doi.org/10.1021/jp410562u | J. Phys. Chem. C 2014, 118, 1843−1855

Table 3. Electronic Couplings for D*A → D $^{+}$A^{-} at the M06HF/6-31G* Level (meV)

systems	V_{CT1}	V_{CT2}
PCPDTBT-IC$_{60}$BM	24.00	17.52
PCPDTBT-bisC$_{70}$BM	27.50	54.02
PCPDTBT-PC$_{60}$BM	22.67	18.59
PCPDTBT-PC$_{70}$BM	22.80	40.08
PCPDTBT-F$_9$	21.96	13.41
PCPDTBT-F$_{16}$	19.90	16.61
PCPDTBT-F$_1$	22.03	9.42
PCPDTBT-F$_{33}$	21.68	13.65
PCPDTBT-F$_2$	23.21	10.88
PCPDTBT-F$_{12}$	23.94	9.54

from the Marcus formula (eq 1). Before proceeding, it is noted that the absolute values of ΔG and λ are very close for several blends, and the corresponding exciton dissociations should be barrierless reactions with the maximum rates. This property can also be used to explain the experimental observation from Jarzab et al.,[8] in which the emission spectra of PCPDTBT in the blend with PC$_{60}$BM have a slight blue-shift compared to that of pure PCPDTBT. This blue shift may come from the upper adiabatic potential well emission, as shown in Figure 5 by the dashed line, because its energy is higher than the adiabatic excitation energy of PCPDTBT due to the interaction between D*A and D^{+}A^{-} states.

Table 4 lists the calculated rates of exciton dissociation for the two channels. For the blends with $\Delta G \approx -\lambda$, as expected,

Table 4. Exciton Dissociation Rates (s^{-1})

systems	k_{L-L}	k_{L-L+1}
PCPDTBT-IC$_{60}$BM	1.90×10^{10}	7.66×10^{6}
PCPDTBT-bisC$_{70}$BM	7.17×10^{11}	1.75×10^{12}
PCPDTBT-PC$_{60}$BM	8.28×10^{11}	4.95×10^{11}
PCPDTBT-PC$_{70}$BM	7.78×10^{11}	2.10×10^{12}
PCPDTBT-F$_9$	6.41×10^{11}	4.06×10^{11}
PCPDTBT-F$_{16}$	2.36×10^{11}	2.52×10^{11}
PCPDTBT-F$_1$	7.83×10^{11}	1.27×10^{11}
PCPDTBT-F$_{33}$	7.52×10^{11}	2.58×10^{11}
PCPDTBT-F$_2$	8.69×10^{11}	1.74×10^{11}
PCPDTBT-F$_{12}$	8.98×10^{11}	1.19×10^{11}

the rates are quite large, and the PCPDTBT-IC$_{60}$BM has the smallest rate caused by the positive driving force. However, the rate for PCPDTBT-bisC$_{70}$BM is still large, although its driving force is not close to the reorganization energy because of large electronic coupling. Experimentally, the exciton dissociation rate for PCPDTBT-PC$_{60}$BM has been estimated to be larger than 1.0×10^{11} s^{-1} (10 ps).[8,109] The calculated rate is 1.30×10^{12} s^{-1}, which is consistent with experimental observation. We thus conclude that for most tested fullerene derivatives except IC$_{60}$BM and bisC$_{70}$BM their driving forces and reorganization energies nearly approach the optimized ones, and the further enhancement of exciton dissociation rates is to optimize the interface geometries to make the electronic coupling as large as possible.

4. CHARGE RECOMBINATION TO THE TRIPLET STATE

As the bound electron−hole pair in the CT state arrives at a thermal equilibrium distribution, it may decay by the radiation and nonradiation processes. Here, we consider the nonradiation process via the triplet state of the PCPDTBT, and its recombination rate can be obtained with a similar method used in the exciton dissociation; however, the corresponding initial and final states are D^{+}A^{-} and ^{3}DA states, respectively.

Table 5 lists the reorganization energies obtained from the equilibrium and nonequilibrium solvent models. The same as

Table 5. Reorganization Energies for D^{+}A^{-} → ^{3}DA from Two Methods (eV)

	equilibrium solvent			nonequilibrium solvent
systems	λ_{in}	λ_s	λ_1	λ_2
PCPDTBT-IC$_{60}$BM	0.3333	0.2956	0.6289	0.6366
PCPDTBT-bisC$_{70}$BM	0.3483	0.2945	0.6428	0.6440
PCPDTBT-PC$_{60}$BM	0.3273	0.2945	0.6218	0.6400
PCPDTBT-PC$_{70}$BM	0.3459	0.2824	0.6283	0.6540
PCPDTBT-F$_9$	0.3273	0.2919	0.6192	0.6390
PCPDTBT-F$_{16}$	0.3272	0.2919	0.6191	0.6383
PCPDTBT-F$_1$	0.3270	0.2919	0.6189	0.6385
PCPDTBT-F$_{33}$	0.3283	0.2919	0.6202	0.6400
PCPDTBT-F$_2$	0.3305	0.2919	0.6224	0.6416
PCPDTBT-F$_{12}$	0.3307	0.2919	0.6226	0.6415

the case for exciton dissociation, two approaches again predict consistent results, manifesting that the four-point model together with nonequilibrium solvent model should be a reliable method to calculate the total reorganization energy. Meanwhile, the reorganization energies are close to one another for all ten blends. However, the internal reorganizations are larger than the solvent ones, which is opposite to the case of exciton dissociation. This phenomenon may be explained by a larger geometric change from D^{+} to ^{3}D than that to D*.

The driving forces correspond to the negative values of ΔG of eq 2 with replacement of E_{00} by the optimized triplet-state energy of PCPDTBT (1.08 eV). Table 6 lists the calculated driving forces. All of the obtained driving forces have negative values, manifesting that the charge recombination is energetically feasible, and the driving forces for PC$_{60}$BM and PC$_{70}$BM blends are nearly the same, coinciding well with an experimental observation.[4] It is noted that the energy gap between the exciton state and triplet state is dominantly determined by the PCPDTBT; therefore, the CT state energies are extremely important to determine the driving forces for both exciton dissociation and charge recombination because the sum of two driving forces exactly equals this energy gap. For instance, the F$_{16}$ blend has a maximal drive force for exciton dissociation, and its driving force for charge recombination becomes the smallest.

The calculations of the electronic coupling for the charge recombination meet more challenges compared with those for exciton dissociation because the triplet state has a spin flip and the RTM cannot be straightforwardly used. Fortunately, the recently proposed constrained DFT[110] can be applied to determine the D^{+}A^{-} and ^{3}DA states, and the TM method is thus applicable to determine the couplings. We calculate the electronic couplings from the NWchem package,[111] and the results are listed in Table 6.

The rates predicted from eq 1 are also listed in Table 6. The detailed comparison reveals that the blends with IC$_{60}$BM and bisPC$_{70}$BM have the largest recombination rates, mainly caused by the large driving forces, and the blends of PC$_{60}$BM and

dx.doi.org/10.1021/jp410562u | J. Phys. Chem. C 2014, 118, 1843−1855

Table 6. Driving Forces ΔG_{CR} (eV), Electronic Couplings (meV), and Rates (s^{-1}) for Charge Recombination

systems	ΔG_{CR}	$V_{D+A-\rightarrow {}^3DA}$	$k_{D+A-\rightarrow {}^3DA}$	$V^3_{(D+A-)\rightarrow {}^3DA}$	$k^3_{(D+A-)\rightarrow {}^3DA}$
PCPDTBT-$IC_{60}BM$	−1.125	20.82	5.56×10^{11}	17.28	1.07×10^{10}
PCPDTBT-bis$C_{70}BM$	−1.260	44.23	9.87×10^{11}	51.61	1.22×10^{10}
PCPDTBT-$PC_{60}BM$	−1.124	19.88	3.20×10^{10}	63.50	1.57×10^{11}
PCPDTBT-$PC_{70}BM$	−1.123	2.57	5.76×10^{8}	0.79	3.22×10^{7}
PCPDTBT-F_9	−1.098	2.56	4.97×10^{8}	20.04	2.20×10^{10}
PCPDTBT-F_{16}	−0.898	22.66	1.58×10^{9}	20.40	1.96×10^{11}
PCPDTBT-F_1	−1.130	6.23	3.38×10^{9}	20.43	1.44×10^{10}
PCPDTBT-F_{33}	−1.115	2.88	7.98×10^{8}	20.88	1.93×10^{10}
PCPDTBT-F_2	−1.110	2.23	4.34×10^{8}	21.02	2.16×10^{10}
PCPDTBT-F_{12}	−1.105	1.70	3.25×10^{8}	22.35	2.61×10^{10}

$PC_{70}BM$ have different electronic couplings although they have similar driving forces and reorganization energies, leading to 2 orders of magnitude different rates. Experimentally, the observed rate of the CT state in the PCPDTBT-$PC_{60}BM$ is about 2.20×10^9 s^{-1} (450 ps). The calculated value of 3.20×10^{10} s^{-1} is obviously larger. However, it is noted that the rate for the $PC_{70}BM$ blend (5.76×10^8 s^{-1}) is indeed smaller than 2.20×10^9 s^{-1}. It is thus expected that the experimental interface geometry may be different from the present one because the electronic couplings are sensitive to the interface geometries of blends. Further tracking into the average electronic coupling of the blend with $IC_{60}BM$ needs to find a variety of possible interface geometries. However, the value of driving force is about six times smaller than the reorganization energy, and the rate will decrease with decreasing temperature. Therefore, these recombination effects should be much smaller than the radiative effect, which may be the reason that the lifetime of the CT state does not depend on the temperatures observed in the experiment.[8] In all, most of these rates are about 2 to 3 orders of magnitude smaller than those of exciton dissociation because these recombinations are in the Marcus normal regime. Except the $IC_{60}BM$ and bis$PC_{70}BM$, it is expected that other fullerene derivatives should be good acceptors because the recombination rates to the triplet states of PCPDTBT are much smaller than the exciton dissociation ones, and the blend with F_{16} may have the lowest open-circuit voltage.

It is noted that the triplet CT state $^3(D^+A^-)$ may be formed by the bimolecular recombination of free electrons and holes.[24,41] Succeedingly, the bounded electron−hole pairs in the $^3(D^+A^-)$ states can also recombine to the ^{3}DA states. In this case, the only differences from $D^+A^- \rightarrow {}^3$DA are electronic couplings. Thus, we calculate the electronic couplings from the TM model in the modified NWchem package,[111] and the results are listed in Table 6. It is seen that most of the electronic couplings for these triplet to triplet recombinations are obviously larger than those for singlet to triplet ones, and the resulting rates $k^3_{(D+A-)\rightarrow {}^3DA}$ are about 10^{10} s^{-1}. Therefore, once the triplet CT states are formed, their recombination to the triplet state of PCPDTBT cannot be neglected because the recombination rates have orders similar to exciton dissociation ones.

5. CONCLUDING REMARKS

We have theoretically predicted the exciton dissociation rates and charge recombination rates to triplet states in the blends of PCPDTBT with ten different fullerene derivatives. The calculated accuracy of driving force, electronic coupling, and internal and external reorganization energies entering the Marcus rate expression are discussed by comparing with experimental spectra. In the Rehm−Weller equation for the calculation of driving force, it is found that the Hirshfeld and NPA charge distributions can correctly describe the Coulomb interaction between the donor and acceptor. In addition, the calculated AEA energies for all tested fullerene derivatives have a good linear relationship with experimental ones, and the estimated driving force from the calculated AEA is reasonable because the obtained energy of the charge transfer state is consistent with experimental florescence. The possible reason for lower experimental AEA may be from the aggregate effect. In the calculation of reorganization energy, both the approaches from the equilibrium and nonequilibrium solvent models are used, and the predicted total reorganization is surprisingly consistent, manifesting that the four-point model together with the nonequilibrium solvent may predict a reasonable value can be extensively used in other systems.

In the tested fullerene derivatives, the values of reorganization energies and driving forces for exciton dissociations are very close except $IC_{60}BM$ and bis$PC_{70}BM$. Therefore, those values are nearly optimized ones, and the exciton dissociations are barrierless reactions. The predicted rate agrees with the experimental value very well. It is thus expected that the optimized interface geometries with larger electronic couplings for those blends become important for the further enhancement of exciton dissociation rates.

For the charge recombination, however, the reorganization energies are explicitly larger than both the exciton dissociation ones and driving forces. The predicted rates are two times smaller than those for exciton dissociations, consistent with experimental observation. However, the recombination rates from the triplet charge transfer states have an order of magnitude similar to the exciton dissociations. Therefore, the triplet charge recombinations are the dominant annihilation channel, which should be suppressed in the present blends to get the high-energy conversion efficiency.

■ ASSOCIATED CONTENT

Supporting Information

Figures S1−S7. This material is available free of charge via the Internet at http://pubs.acs.org.

■ AUTHOR INFORMATION

Corresponding Author

*E-mail: yizhao@xmu.edu.cn.

Notes

The authors declare no competing financial interest.

■ ACKNOWLEDGMENTS

This work is partially supported by the National Science Foundation of China (Grant Nos. 21073146, 21133007, 91333101) and the National Basic Research Program of China (Grant No. 2011CB808501).

■ REFERENCES

(1) Chen, J. W.; Cao, Y. Development of Novel Conjugated Donor Polymers for High-Efficiency Bulk-Heterojunction Photovoltaic Devices. *Acc. Chem. Res.* **2009**, *42*, 1709−1718.
(2) Boudreault, P. L. T.; Najari, A.; Leclerc, M. Processable Low-Bandgap Polymers for Photovoltaic Applications. *Chem. Mater.* **2011**, *23*, 456−469.
(3) Risko, C.; McGehee, M. D.; Brédas, J. L. A Quantum-Chemical Perspective into Low Optical-Gap Polymers for Highly-Efficient Organic Solar Cells. *Chem. Sci.* **2011**, *2*, 1200−1218.
(4) Mühlbacher, D.; Scharber, M.; Morana, M.; Zhu, Z. G.; Gaudiana, D. W. R.; Brabec, C. High Photovoltaic Performance of a Low-Bandgap Polymer. *Adv. Mater.* **2006**, *18*, 2884−2889.
(5) Peet, J.; Kim, J. Y.; Coates, N. E.; Ma, W. L.; Moses, D.; Heeger, A. J.; Bazan, G. C. Efficiency Enhancement in Low-Bandgap Polymer Solar Cells by Processing with Alkane Dithiols. *Nat. Mater.* **2007**, *6*, 497−500.
(6) Lee, J. K.; Ma, W. L.; Brabec, C. J.; Yuen, J.; Moon, J. S.; Kim, J. Y.; Lee, K.; Bazan, G. C.; Heeger, A. J. Processing Additives for Improved Efficiency from Bulk Heterojunction Solar Cells. *J. Am. Chem. Soc.* **2008**, *130*, 3619−3623.
(7) Nuzzo, D. D.; Aguirre, A.; Shahid, M.; Gevaerts, V. S.; Meskers, S. C. J.; Janssen, R. A. J. Improved Film Morphology Reduces Charge Carrier Recombination into the Triplet Excited State in a Small Bandgap Polymer-Fullerene Photovoltaic Cell. *Adv. Mater.* **2010**, *22*, 4321−4324.
(8) Jarzab, D.; Cordella, F.; Gao, J.; Scharber, M.; Egelhaaf, H. J.; Loi, M. A. Low-Temperature Behaviour of Charge Transfer Excitons in Narrow-Bandgap Polymer-Based Bulk Heterojunctions. *Adv. Energy Mater.* **2011**, *1*, 604−609.
(9) Hwang, I. W.; Soci, C.; Moses, D.; Zhu, Z. G.; Waller, D.; Gaudiana, R.; Brabec, C. J.; Heeger, A. J. Ultrafast Electron Transfer and Decay Dynamics in a Small Band Gap Bulk Heterojunction Material. *Adv. Mater.* **2007**, *19*, 2307−2312.
(10) Hwang, I. W.; Cho, S.; Kim, J. Y.; Lee, K.; Coates, N. E.; Moses, D.; Heeger, A. J. Carrier Generation and Transport in Bulk Heterojunction Films Processed with 1,8-Octanedithiol as A Processing Additive. *J. Appl. Phys.* **2008**, *104*, 033706.
(11) Lenes, M.; Morana, M.; Brabec, C. J.; Blom, P. W. M. Recombination-Limited Photocurrents in Low Bandgap Polymer/Fullerene Solar Cells. *Adv. Funct. Mater.* **2009**, *19*, 1106−1111.
(12) Piliegoa, C.; Loi, M. A. Charge Transfer State in Highly Efficient Polymer-Fullerene Bulk Heterojunction Solar Cells. *J. Mater. Chem.* **2012**, *22*, 4141−4150.
(13) Koerner, C.; Ziehlke, H.; Gresser, R.; Fitzner, R.; Reinold, E.; Bäuerle, P.; Leo, K.; Riede, M. Temperature Activation of the Photoinduced Charge Carrier Generation Efficiency in Quaterthiophene:C_{60} Mixed Films. *J. Phys. Chem. C* **2012**, *116*, 25097−25105.
(14) Westenhoff, S.; Howard, I. A.; Hodgkiss, J. M.; Kirov, K. R.; Bronstein, H. A.; Williams, C. K.; Greenham, N. C.; Friend, R. H. Charge Recombination in Organic Photovoltaic Devices with High Open-Circuit Voltages. *J. Am. Chem. Soc.* **2008**, *130*, 13653−13658.
(15) Liedtke, M.; Sperlich, A.; Kraus, H.; Baumann, A.; Deibel, C.; Wirix, M. J. M.; Loos, J.; Cardona, C. M.; Dyakonov, V. Triplet Exciton Generation in Bulk-Heterojunction Solar Cells Based on Endohedral Fullerenes. *J. Am. Chem. Soc.* **2011**, *133*, 9088−9094.
(16) Schlenker, C. W.; Chen, K. S.; Yip, H. L.; Li, C. Z.; Bradshaw, L. R.; Ochsenbein, S. T.; Ding, F. Z.; Li, X. S. S.; Gamelin, D. R.; Jen, A. K. Y.; et al. Polymer Triplet Energy Levels Need Not Limit Photocurrent Collection in Organic Solar Cells. *J. Am. Chem. Soc.* **2012**, *134*, 19661−19668.
(17) Veldman, D.; Ipek, O.; Meskers, S. C. J.; Sweelssen, J.; Koetse, M. M.; Veenstra, S. C.; Kroon, J. M.; van Bavel, S. S.; Loos, J.; Janssen, R. A. J. Compositional and Electric Field Dependence of the Dissociation of Charge Transfer Excitons in Alternating Polyfluorene Copolymer/Fullerene Blends. *J. Am. Chem. Soc.* **2008**, *130*, 7721−7735.
(18) Veldman, D.; Meskers, S. C. J.; Janssen, R. A. J. The Energy of Charge-Transfer States in Electron DonorCAcceptor Blends: Insight into the Energy Losses in Organic Solar Cells. *Adv. Funct. Mater.* **2009**, *19*, 1939−1948.
(19) Giebink, N. C.; Lassiter, B. E.; Wiederrecht, G. P.; Wasielewski, M. R.; Forrest, S. R. Ideal Diode Equation for Organic Heterojunctions. II. The Role of Polaron Pair Recombination. *Phys. Rev. B* **2010**, *82*, 155306.
(20) Dutton, G. J.; Jin, W.; Reutt-Robey, J. E.; Robey, S. W. Ultrafast Charge-Transfer Processes at An Oriented Phthalocyanine/C_{60} Interface. *Phys. Rev. B* **2010**, *82*, 073407.
(21) Deschler, F.; Como, E. D.; Limmer, T.; Tautz, R.; Godde, T.; Bayer, M.; von Hauff, E.; Yilmaz, S.; Allard, S.; Scherf, U.; et al. Reduced Charge Transfer Exciton Recombination in Organic Semiconductor Heterojunctions by Molecular Doping. *Phys. Rev. Lett.* **2011**, *107*, 127402.
(22) Distler, A.; Kutka, P.; Sauermann, T.; Egelhaaf, H. J.; Guldi, D. M.; Nuzzo, D. D.; Meskers, S. C. J.; Janssen, R. A. J. Effect of PCBM on the Photodegradation Kinetics of Polymers for Organic Photovoltaics. *Chem. Mater.* **2012**, *23*, 4397−4405.
(23) Koster, L. J. A.; Shaheen, S. E.; Hummelen, J. C. Pathways to a New Efficiency Regime for Organic Solar Cells. *Adv. Energy Mater.* **2012**, *2*, 1246−1253.
(24) Rao, A.; Chow, P. C. Y.; Gélinas, S.; Schlenker, C. W.; Li, C. Z.; Yip, H. L.; Jen, A. K. Y.; Ginger, D. S.; Friend, R. H. The Role of Spin in The Kinetic Control of Recombination in Organic Photovoltaics. *Nature* **2013**, *500*, 435−439.
(25) Marcus, R. A. On The Theory of Oxidation-Reducation Reactions involving Electron Transfer. V. Comparison and Properties of Electrochemical and Chemical Rate Constants. *J. Phys. Chem.* **1963**, *67*, 853−857.
(26) Marcus, R. A.; Sutin, N. Electron Transfers in Chemistry and Biology. *Biochim. Biophys. Acta* **1985**, *811*, 265−322.
(27) Zhao, Y.; Liang, W. Z. Charge Transfer in Organic Molecules for Solar Cells: theoretical perspective. *Chem. Soc. Rev.* **2012**, *41*, 1075−1087.
(28) Kawatsu, T.; Coropceanu, V.; Ye, A. J.; Brédas, J. L. Quantum-Chemical Approach to Electronic Coupling: Application to Charge Separation and Charge Recombination Pathways in a Model Molecular Donor-Acceptor System for Organic Solar Cells. *J. Phys. Chem. C* **2008**, *112*, 3429−3433.
(29) Yi, Y. P.; Coropceanu, V.; Brédas, J. L. Exciton-Dissociation and Charge-Recombination Processes in Pentacene/C_{60} Solar Cells: Theoretical Insight into the Impact of Interface Geometry. *J. Am. Chem. Soc.* **2009**, *131*, 15777−15783.
(30) Grancini, G.; Polli, D.; Fazzi, D.; Gonzalez, J. C.; Cerullo, G.; Lanzani, G. Transient Absorption Imaging of P_3HT:PCBM Photovoltaic Blend: Evidence For Interfacial Charge Transfer State. *J. Phys. Chem. Lett.* **2011**, *2*, 1099−1105.
(31) McMahon, D. P.; Cheung, D. L.; Troisi, A. Why Holes and Electrons Separate So Well in Polymer/Fullerene Photovoltaic Cells. *J. Phys. Chem. Lett.* **2011**, *2*, 2737−2741.
(32) Lee, J.; Vandewal, K.; Yost, S. R.; Bahlke, M. E.; Goris, L.; Baldo, M. A.; Manca, J. V.; Voorhis, T. V. Charge Transfer State Versus Hot Exciton Dissociation in Polymer-Fullerene Blended Solar Cells. *J. Am. Chem. Soc.* **2010**, *132*, 11878−11880.
(33) Liu, T.; Cheung, D. L.; Troisi, A. Structural Variability and Dynamics of The P_3HT/PCBM Interface and Its Effects on The Electronic Structure and The Charge-Transfer Rates in Solar Cells. *Phys. Chem. Chem. Phys.* **2011**, *13*, 21461−21470.
(34) Yi, Y. P.; Coropceanu, V.; Brédas, J. L. A Comparative Theoretical Study of Exciton-Dissociation and Charge-Recombination Processes in Oligothiophene/Fullerene and Oligothiophene/Peryle-

nediimide Complexes for Organic Solar Cells. *J. Mater. Chem.* **2011**, *21*, 1479−1486.
(35) Fazzi, D.; Grancini, G.; Maiuri, M.; Brida, D.; Cerull, G.; Lanzani, G. Ultrafast Internal Conversion in A Low Band Gap Polymer for Photovoltaics: Experimental and Theoretical Study. *Phys. Chem. Chem. Phys.* **2012**, *14*, 6367−6374.
(36) Zhang, W. W.; Chen, X.; Liang, W. Z.; Zhao, Y. Electron Transfer Pathways in the Z-schematic Donor-Donor-Acceptor Organic Solar Cells. *Commun. Comput. Chem.* **2013**, *1*, 132−144.
(37) Rehm, D.; Weller, A. Kinetics of Fluorescence Quenching by Electron Transfer and H-atom Transfer. *Israel J. Chem.* **1970**, *8*, 259−271.
(38) Nelsen, S. F.; Blackstock, S. C.; Kim, Y. Estimation of Inner Shell Marcus Terms for Amino Nitrogen Compounds by Molecular Orbital Calculations. *J. Am. Chem. Soc.* **1987**, *109*, 677−682.
(39) Banerji, N.; Cowan, S.; Leclerc, M.; Vauthey, E.; Heeger, A. J. Exciton Formation, Relaxation, and Decay in PCDTBT. *J. Am. Chem. Soc.* **2010**, *132*, 17459−17470.
(40) Horward, I. A.; Mauer, R.; Meister, M.; Laquai, F. Effect of Morphology on Ultrafast Free Carrier Generation in Polythiophene:-Fullerene Organic Solar Cells. *J. Am. Chem. Soc.* **2010**, *132*, 14866−14876.
(41) Bakulin, A. A.; Rao, A.; Pavelyev, V. G.; van Loosdrecht, P. H. M.; Pshenichnikov, M. S.; Niedzialek, D.; Cornil, J.; Beljonne, D.; Friend, R. H. The Role of Driving Energy and Delocalized States for Charge Separation in Organic Semiconductors. *Science* **2012**, *335*, 1340−1344.
(42) Grancini, G.; Maiuri, M.; Fazzi, D.; Petrozza, A.; Egelhaaf, H. J.; Brida, D.; Cerullo, G.; Lanzani, G. Hot Exciton Dissociation in Polymer Solar Cells. *Nat. Mater.* **2013**, *12*, 29−33.
(43) Deibel, C.; Strobel, T.; Dyakonov, V. Role of the Charge Transfer State in Organic Donor-Acceptor Solar Cells. *Adv. Mater.* **2010**, *22*, 4097−4111.
(44) Koster, L. J. A.; Smits, E. C. P.; Mihailetchi, V. D.; Blom, P. W. M. Device model for the operation of polymer/fullerene bulk heterojunction solar cells. *Phys. Rev. B* **2005**, *72*, 085205.
(45) Zhong, X. X.; Zhao, Y. Non-Markovian Stochastic Schrödinger Equation at Finite Temperatures for Charge Carrier Dynamics in Organic Crystals. *J. Chem. Phys.* **2013**, *138*, 014111.
(46) Hilczer, M.; Tachiya, M. Unified Theory of Geminate and Bulk Electron-Hole Recombination in Organic Solar Cells. *J. Phys. Chem. C* **2010**, *114*, 6808−6813.
(47) Yu, G.; Gao, J.; Hummelen, J. C.; Wudl, F.; Heeger, A. J. Polymer Photovoltaic Cells: Enhanced Efficiencies via A Network of Internal Donor-Acceptor Heterojunctions. *Science* **1995**, *270*, 1789−1791.
(48) Troshin, P. A.; Hoppe, H.; Renz, J.; Egginger, M.; Mayorova, J. Y.; Goryachev, A. E.; Peregudov, A. S.; Lyubovskaya, R. N.; Gobsch, G.; Sariciftci, N. S.; et al. Material Solubility-Photovoltaic Performance Relationship in the Design of Novel Fullerene Derivatives for Bulk Heterojunction Solar Cells. *Adv. Funct. Mater.* **2009**, *19*, 779−788.
(49) Zhao, G. J.; He, Y. J.; Xu, Z.; Hou, J. H.; Zhang, M. J.; Min, J.; Chen, H. Y.; Ye, M. F.; Hong, Z.; Yang, Y.; Li, Y. F. Effect of Carbon Chain Length in the Substituent of PCBM-like Molecules on Their Photovoltaic Properties. *Adv. Funct. Mater.* **2010**, *20*, 1480−1487.
(50) He, Y. J.; Li, Y. F. Fullerene Derivative Acceptors for High Performance Polymer Solar Cells. *Phys. Chem. Chem. Phys.* **2011**, *13*, 1970−1983.
(51) Clarke, T.; Ballantyne, A.; Jamieson, F.; Brabec, C.; Nelson, J.; Durrant, J. Transient Absorption Spectroscopy of Charge Photogeneration Yields and Lifetimes in a Low Bandgap Polymer/Fullerene Film. *Chem. Commun.* **2009**, *89*, 89−91.
(52) Kettle, J.; Rees, A.; Brousseau, E. B.; Horie, M. Low-Temperature Thermal Nanoimprint Lithography of Anti-feflective Structures for Flexible Low Band Gap Organic Solar Cells. *J. Phys. D: Appl. Phys.* **2013**, *46*, 105102.
(53) Koppe, M.; Egelhaaf, H. J.; Dennler, G.; Scharber, M. C.; Brabec, C. J.; Schilinsky, P.; Hoth, C. N. Near IR Sensitization of Organic Bulk Heterojunction Solar Cells: Towards Optimization of the Spectral Response of Organic Solar Cells. *Adv. Funct. Mater.* **2010**, *20*, 338−346.
(54) Namkoong, G.; Boland, P.; Lee, K.; Dean, J. Design of Organic Tandem Solar Cells using PCPDTBT:$PC_{61}BM$ and P_3HT:$PC_{71}BM$. *J. Appl. Phys.* **2010**, *107*, 124515.
(55) Albrecht, S.; Schäfer, S.; Lange, I.; Yilmaz, S.; Dumsch, I.; Allard, S.; Scherf, U.; Hertwig, A.; Neher, D. Light Management in PCPDTBT:$PC_{70}BM$ Solar Cells: A Comparison of Standard and Inverted Device Structures. *Org. Electron* **2012**, *13*, 615−622.
(56) Pandey, L.; Doiron, C.; Sears, J. S.; Brédas, J. L. Lowest Excited States and Optical Absorption Spectra of Donor-Acceptor Copolymers for Organic Photovoltaics: A New Picture Emerging from Tuned Long-Range Corrected Density Functionals. *Phys. Chem. Chem. Phys.* **2012**, *14*, 14243−14248.
(57) Fischer, F. S. U.; Tremel, K.; Saur, A. K.; Link, S.; Kayunkid, N.; Brinkmann, M.; Herrero-Carvajal, D.; Navarrete, J. T. L.; Delgado, M. C. R.; Ludwigs, S. Influence of Processing Solvents on Optical Properties and Morphology of a Semicrystalline Low Bandgap Polymer in the Neutral and Charged States. *Macromolecules* **2013**, *46*, 4924−4931.
(58) Tautz, R.; Como, E. D.; Wiebeler, C.; Soavi, G.; Dumsch, I.; Fröhlich, N.; Grancini, G.; Allard, S.; Scherf, U.; Cerullo, G.; et al. Charge Photogeneration in Donor-Acceptor Conjugated Materials: Influence of Excess Excitation Energy and Chain Length. *J. Am. Chem. Soc.* **2013**, *135*, 4282−4290.
(59) Wiebeler, C.; Tautz, R.; Feldmann, J.; von Hauff, E.; Como, E. D.; Schumacher, S. Spectral Signatures of Polarons in Conjugated Copolymers. *J. Phys. Chem. B* **2013**, *117*, 4454−4460.
(60) Yang, J. H.; Zhang, W. W.; Si, Y. B.; Zhao, Y. Intramolecular Electronic Couplings in Class II/III Organic Mixed-Valence Systems of Bis(1,4-dimethoxybenzene). *J. Phys. Chem. B* **2012**, *116*, 14126−14135.
(61) Yanai, T.; P.Tew, D.; Handy, N. C. A New Hybrid Exchange-Correlation Functional using the Coulomb-Attenuating Method (CAM-B3LYP). *Chem. Phys. Lett.* **2004**, *393*, 51−57.
(62) Chai, J. D.; Gordon, M. H. Long-Range Corrected Hybrid Density Functionals with Damped Atom−Atom Dispersion Corrections. *Phys. Chem. Chem. Phys.* **2008**, *10*, 6615−6620.
(63) Chiew, E. K.; Yahaya, M.; Othman, A. P. Electrical Characterization of P3HT/PCBM Bulk Heterojunction Organic Solar Cell. *Int. J. Comput. Mater. Sci. Eng.* **2012**, *1*, 1250004.
(64) Zhu, J. F.; Zeng, B. Q.; Kim, R. S.; Wu, Z. Light Concentration in Polymer Bulk Heterojunction Solar Cells with Plasmonic Nanoparticles. *Proc. SPIE* **2012**, *8333*, 83331C.
(65) Frisch, M. J.; Trucks, G. W.; Schlegel, H. B.; Scuseria, G. E.; Robb, M. A.; Cheeseman, J. R.; Scalmani, G.; Barone, B. M. V.; Petersson, G. A.; Nakatsuji, H.; et al. *Gaussian 09*, Revision B.01; Gaussian, Inc.: Wallingford, CT, 2010.
(66) Maurano, A.; Hamilton, R.; Shuttle, C. G.; Ballantyne, A. M.; Nelson, J.; O'Regan, B.; Zhang, W. M.; McCulloch, I.; Azimi, H.; Morana, M.; et al. Recombination Dynamics as a Key Determinant of Open Circuit Voltage in Organic Bulk Heterojunction Solar Cells: A Comparison of Four Different Donor Polymers. *Adv. Mater.* **2010**, *22*, 4987−4992.
(67) Aygül, U.; Peisert, H.; Frisch, J.; Vollmer, A.; Koch, N.; Chassé, T. Electronic Properties of Interfaces between PCPDTBT and Prototypical Electrodes Studied by Photoemission Spectroscopy. *Chem. Phys. Chem.* **2011**, *12*, 2345−2351.
(68) Andreoni, W. Computational Approach to the Physical Chemistry of Fullerenes and Their Derivatives. *Annu. Rev. Phys. Chem.* **1998**, *49*, 405−439.
(69) Tuladhar, S. M.; Poplavskyy, D.; Choulis, S. A.; Durrant, J. R.; Bradley, D. D. C.; Nelson, J. Ambipolar Charge Transport in Films of Methanofullerene and Poly(phenylenevinylene)/Methanofullerene Blends. *Adv. Funct. Mater.* **2005**, *15*, 1171−1182.
(70) Hoke, E. T.; Sachs-Quintana, I. T.; Lloyd, M. T.; Kauvar, I.; Mateker, W. R.; Nardes, A. M.; Peters, C. H.; Kopidakis, N.; McGehee, M. D. The Role of Electron Affinity in Determining Whether

Fullerenes Catalyze or Inhibit Photooxidation of Polymers for Solar Cells. *Adv. Energy Mater.* **2012**, *2*, 1351−1357.
(71) Liu, T.; Troisi, A. Absolute Rate of Charge Separation and Recombination in a Molecular Model of the P_3HT/PCBM Interface. *J. Phys. Chem. C* **2011**, *115*, 2406−2415.
(72) Oevering, H.; Paddon-Row, M. N.; Heppener, M.; Oliver, A. M.; Cotsaris, E.; Verhoeven, J. W.; Hush, N. S. Long-range Photoinduced Through-bond Electron Transfer and Radiative Recombination via Rigid Nonconjugated Bridges: Distance and Solvent Dependence. *J. Am. Chem. Soc.* **1987**, *109*, 3258−3269.
(73) Veldman, D.; Chopin, S. M. A.; Meskers, S. C. J.; Janssen, R. A. J. Enhanced Intersystem Crossing via a High Energy Charge Transfer State in a Perylenediimide-Perylenemonoimide Dyad. *J. Phys. Chem. A* **2008**, *112*, 8617−8632.
(74) Williams, R. M.; Koeberg, M.; Lawson, J. M.; An, Y. Z.; Rubin, Y.; Paddon-Row, M. N.; Verhoeven, J. W. Photoinduced Electron Transfer to C_{60} across Extended 3- and 11-Bond Hydrocarbon Bridges: Creation of a Long-Lived Charge-Separated State. *J. Org. Chem.* **1996**, *61*, 5055−5062.
(75) Karsten, B. P.; Bouwer, R. K. M.; Hummelen, J. C.; Williams, R. M.; Janssen, R. A. J. Charge Separation and (Triplet) Recombination in Diketopyrrolopyrrole-Fullerene Triads. *Photochem. Photobiol. Sci.* **2010**, *9*, 1055−1065.
(76) Martin, F.; Zipse, H. Charge Distribution in the Water Molecule-A Comparison of Methods. *J. Comput. Chem.* **2004**, *26*, 97−105.
(77) Mulliken, R. S. Electronic Population Analysis on LCAO-MO Molecular Wave Functions. II. Overlap Populations, Bond Orders, and Covalent Bond Energies. *J. Chem. Phys.* **1955**, *23*, 1841−1846.
(78) Mulliken, R. S. Criteria for the Construction of Good Self-Consistent-Field Molecular Orbital Wave Functions, and the Significance of LCAO-MO Population Analysis. *J. Chem. Phys.* **1962**, *36*, 3428−3439.
(79) Reed, A. E.; Weinstock, R. B.; Weinhold, F. Natural Population Analysis. *J. Chem. Phys.* **1985**, *83*, 735−746.
(80) Curtiss, A. E. R. L. A.; Weinhold, F. Intermolecular Interactions from a Natural Bond Orbital, Donor-Acceptor Viewpoint. *J. Chem. Phys.* **1988**, *88*, 899−926.
(81) Hirshfeld, F. L. Atomic Charges Derived from Semiempirical Methods. *Theor. Chem. Acc.* **1977**, *44*, 129−138.
(82) Breneman, C. M.; Wiberg, K. B. Determining Atom-Centered Monopoles from Molecular Electrostatic Potentials. The Need for High Sampling Density in Formamide Conformational Analysis. *J. Chem. Phys.* **1990**, *11*, 361−373.
(83) Singh, U. C.; Kollman, P. A. An Approach to Computing Electrostatic Charges for Molecules. *J. Comput. Chem.* **1984**, *5*, 129−145.
(84) Besler, B. H.; Merz, K. M.; Kollman, P. A. Atomic Charges Derived from Semiempirical Methods. *J. Comput. Chem.* **1990**, *11*, 431−439.
(85) Gadisa, A.; Svensson, M.; Andersson, M. R.; Inganäs, O. Correlation between Oxidation Potential and Open-Circuit Voltage of Composite Solar Cells based on Blends of Polythiophenes/Fullerene Derivative. *Appl. Phys. Lett.* **2004**, *84*, 1609−1611.
(86) Mutolo, K. L.; Mayo, E. I.; Rand, B. P.; Forrest, S. R.; Thompson, M. E. Enhanced Open-Circuit Voltage in Subphthalocyanine/C_{60} Organic Photovoltaic Cells. *J. Am. Chem. Soc.* **2006**, *128*, 8108−8109.
(87) Vandewal, K.; Gadisa, A.; Oosterbaan, W. D.; Bertho, S.; Banishoeib, F.; Severen, I. V.; Lutsen, L.; Cleij, T. J.; Vanderzande, D.; Manca, J. V. The Relation Between Open-Circuit Voltage and the Onset of Photocurrent Generation by Charge-Transfer Absorption in Polymer: Fullerene Bulk Heterojunction Solar Cells. *Adv. Funct. Mater.* **2008**, *18*, 2064−2070.
(88) Zhang, W. W.; Zhu, W. J.; Liang, W. Z.; Zhao, Y.; Nelsen, S. F. Ab Initio Calculations on the Intramolecular Electron Transfer Rates of a Bis(hydrazine) Radical Cation. *J. Phys. Chem. B* **2008**, *112*, 11079−11086.
(89) Qin, H. M.; Zhong, X. X.; Si, Y. B.; Zhang, W. W.; Zhao, Y. Effect of Group Electronegativity on Electron Transfer in Bis-(hydrazine) Radical Cations. *J. Phys. Chem. A* **2011**, *115*, 3116−3121.
(90) Nelsen, S. F.; Blomgren, F. Estimation of Electron Transfer Parameters from AM1 Calculations. *J. Org. Chem.* **2001**, *66*, 6551−6559.
(91) Matyushov, D. V. Energetics of Electron-Transfer Reactions in Soft Condensed Media. *Acc. Chem. Res.* **2007**, *40*, 294−301.
(92) Marcus, R. A. On the Theory of Oxidation-Reduction Reactions Involving Electron Transfer. I. *J. Chem. Phys.* **1956**, *24*, 966−978.
(93) Bader, R. F. W.; Preston, H. J. T. Determination of the Charge Distribution of Methane by a Method of Density Constraints. *Theor. Chim. Acta* **1970**, *17*, 384−395.
(94) Bader, R. F. W.; Carroll, M. T.; Cheeseman, J. R.; Chang, C. Properties of Atoms in Molecules: Atomic Volumes. *J. Am. Chem. Soc.* **1987**, *109*, 7968−7979.
(95) Caricato, M.; Ingrosso, F.; Mennucci, B.; Sato, H. Electron Transfer in A Radical Ion Pair: Quantum Calculations of the Solvent Reorganization Energy. *J. Phys. Chem. B* **2006**, *110*, 25115−25121.
(96) Hsu, C. P. The Electronic Couplings in Electron Transfer and Excitation Energy Transfer. *Acc. Chem. Res.* **2009**, *42*, 509−518.
(97) Koopmans, T. über die Zuordnung von Wellenfunktionen und Eigenwerten zu den Einzelnen Elektronen Eines Atoms. *Physica* **1934**, *1*, 104−113.
(98) Jordan, K. D.; Paddon-Row, M. N. Analysis of the Interactions Responsible for Long-Range Through-Bond-Mediated Electronic Coupling between Remote Chromophores Attached to Rigid Polynorbornyl Bridges. *Chem. Rev.* **1992**, *92*, 395−410.
(99) Cornil, J.; Beljonne, D.; Calbert, J. P.; Brédas, J. L. Interchain Interactions in Organic π-Conjugated Materials: Impact on Electronic Structure, Optical Response, and Charge Transport. *Adv. Mater.* **2001**, *13*, 1053−1067.
(100) Datta, A.; Mohakud, S.; Pati, S. K. Comparing The Electron and Hole Mobilities in the α and β Phases of Perylene: Role of π-Stacking. *J. Mater. Chem.* **2007**, *17*, 1933−1938.
(101) Farazdel, A.; Dupuis, M.; Clementi, E.; Avitam, A. Electric Field Induced Intramolecular Electron Transfer in Spiro π-Electron Systems and Their Suitability as Molecular Electronic Devices. A Theoretical Study. *J. Am. Chem. Soc.* **1990**, *112*, 4206−4214.
(102) You, Z. Q.; Shao, Y. H.; Hsu, C. P. Calculating Electron Transfer Couplings by The Spin-Flip Approach: Energy Splitting and Dynamical Correlation Effects. *Chem. Phys. Lett.* **2004**, *390*, 116−123.
(103) Si, Y. B.; Zhang, W. W.; Zhao, Y. Theoretical Investigations of Spin-Orbit Coupling and Kinetics in Reaction $W + NH_3 \rightarrow N{\equiv}WH_3$. *J. Phys. Chem. A* **2012**, *116*, 2583−2590.
(104) Cave, R. J.; Newton, M. D. Generalization of The Mulliken-Hush Treatment for The Calculation of Electron Transfer Matrix Elements. *Chem. Phys. Lett.* **1996**, *249*, 15−19.
(105) Valeev, E. F.; Coropceanu, V.; da Silver Filho, D. A.; Salman, S.; Brédas, J. L. Effect of Electronic Polarization on Charge-Transport Parameters in Molecular Organic Semiconductors. *J. Am. Chem. Soc.* **2006**, *128*, 9882−9886.
(106) Zhang, W. W.; Liang, W. Z.; Zhao, Y. Non-Condon Effect on Charge Transport in Dithiophene-Tetrathiafulvalene Crystal. *J. Chem. Phys.* **2010**, *133*, 024501.
(107) Zhang, W. W.; Zhu, W. J.; Liang, W. Z.; Zhao, Y.; Nelsen, S. F. Ab Initio Calculations on the Intramolecular Electron Transfer Rates of a Bis(hydrazine) Radical Cation. *J. Phys. Chem. B* **2008**, *112*, 11079−11086.
(108) Si, Y. B.; Liang, W. Z.; Zhao, Y. Theoretical Prediction of Triplet-Triplet Energy Transfer Rates in a Benzophenone-Fluorene-Naphthalene System. *J. Phys. Chem. C* **2012**, *116*, 12499−12507.
(109) Etzold, F.; Howard, I. A.; Forler, N.; Cho, D. M.; Meister, M.; Mangold, H.; Shu, J.; Hansen, M. R.; Müllen, K.; Laquai, F. The Effect of Solvent Additives on Morphology and Excited-State Dynamics in PCPDTBT:PCBM Photovoltaic Blends. *J. Am. Chem. Soc.* **2012**, *134*, 10569−10583.
(110) Voorhis, T. V.; Kowalczyk, T.; Kaduk, B.; Wang, L. P.; Cheng, C. L.; Wu, Q. The Diabatic Picture of Electron Transfer, Reaction

Barriers, and Molecular Dynamics. *Annu. Rev. Phys. Chem.* **2010**, *61*, 149−170.
(111) Valieva, M.; Bylaska, E. J.; Govind, N.; Kowalski, K.; Straatsma, T. P.; van Dam, H. J. J.; Wang, D.; Nieplocha, J.; Apra, E.; Windus, T. L.; et al. NWChem: A Comprehensive and Scalable Open-Source Solution for Large Scale Molecular Simulations. *Comput. Phys. Commun.* **2010**, *181*, 1477−1489.